Journal of Sound and Vibration (2001) **239**(2), 201–215
doi:10.1006/jsvi.2000.3119, available online at http://www.idealibrary.com on IDEAL®

THE DYNAMIC ANALYSIS OF A MULTISPAN FLUID-CONVEYING PIPE SUBJECTED TO EXTERNAL LOAD

J.-S. Wu and P.-Y. Shih

Institute of Naval Architecture and Marine Engineering, National Cheng-Kung University, Tainan, Taiwan 701, *Republic of China. E-mail: jswu@mail.ncku.edu.tw*

(*Received* 13 *December* 1999, *and in final form* 7 *April* 2000)

Instead of the "functional" mode shapes (defined by the admissible, comparison or eigenfunctions) employed by the classical assumed mode (or modal analysis) method, the lowest several "numerical" (or vector) mode shapes and the associated natural frequencies of a "non-periodic" multispan pipe with the prescribed supporting conditions and filled with the "stationary" fluid (with velocity $U = 0$) are determined by means of the transfer matrix method (TMM). Using the last mode shapes together with the natural frequencies and incorporating with the expansion theorem, the partial differential equation of motion for the infinite degree-of-freedom (d.o.f.) continuous multispan pipe filled with "flowing" fluid (with $U \neq 0$) is converted into a matrix equation. Solving the last matrix equation with the direct integration method gives the dynamic responses of the fluid-conveying pipe. Since the order of the transfer matrix for either each pipe segment or the entire piping system is 4×4, which is independent of the number of the spans for the system, the presented approach is simpler than the existing techniques, particularly for the piping systems with large number of spans. It is also noted that the classical assumed mode (or modal analysis) method is easily applicable only to the special cases where the functions for the approximate mode shapes are obtainable, such as the "single-span" beams or the "periodical" multispan beams (with identical spans and identical constraints). However, the presented "numerical" (or vector) mode method is suitable for many practical engineering problems.

1. INTRODUCTION

The dynamic analyses of a "single-span" pipe that conveys fluid have been extensively performed by many researchers [1–8]. But the literature regarding the dynamic analyses of a "multispan" fluid-conveying pipe (either finite or infinite) is relatively limited [9–12] in spite of the fact that the material for general periodic structures subjected to other kinds of loads (such as moving loads, convected pressure fields, etc.) is abundant [13–18]. From the existing literature, one finds that most of the researchers studied the stability problem of the piping systems [1–7, 9–12], whereas fewer researchers have studied the forced vibration of a fluid-conveying pipe [3, 8, 9, 12]. Most dynamic analyses of a "single-span" piping system are performed using the assumed mode (or modal analysis) method [1–4, 7] or FEM [5, 6], but those of a "periodically supported" fluid-conveying piping system are solved with the wave approach [10–12]. This is because the dynamic equation of motion for any span of the latter system is the same and the amount of computation for the wave approach is independent of the number of spans.

Although the literature regarding "periodical" multispan structures is vast [9–12, 13–15, 17], that relating to the general "non-periodical" ones is rare [16, 18]. The main reason is

0022-460X/01/020201 + 15 $35.00/0

that the wave approach is easily applicable only to periodic structures and not to non-periodic ones. In addition, the conventional FEM can become very laborious when the number of spans is very large. In Refs. [17, 18], the order of the overall property matrices for the whole multispan structure is significantly reduced by using the dynamic stiffness matrices [19] and only one element per span. However, the order of the overall property matrices for the whole structure is yet to increase with the number of spans. This is unlike the transfer matrix method (TMM) [16, 20], in which the order of the overall transfer matrix is kept unchanged. Furthermore, since the dynamic responses obtained from the dynamic-stiffness-matrix method are in the "frequency domain" [17, 18], the last method will not be a suitable approach if the pertinent information required is the dynamic responses in the "time domain" such as the time histories of displacements for certain points of a piping system.

In this paper, the lowest several natural frequencies and the associated normal mode shapes of a non-periodic multispan pipe filled with "stationary" fluid (with velocity $U = 0$) are determined with the TMM [16, 20]. Then by using the foregoing free-vibration-analysis results and the expansion theorem [21], the partial differential equation of motion for a multispan piping system conveying fluid (with velocity $U \neq 0$) and subject to external loads is converted into a matrix equation. Solving the last matrix equation with the direct integration method [22] yields the dynamic responses of the piping system. Comparing with the existing techniques, it is found that the presented approach has the advantage of being more simple, straightforward and practical.

For convenience, the classical assumed mode (or modal analysis) method is called the "functional" mode method and the presented method is the "numerical" (or vector) mode method in this paper. This is because the mode shapes for the assumed mode (or modal analysis) method take the form of admissible functions, comparison functions or eigenfunctions, while those for the presented method cannot be represented by the last functions and must be defined numerically (in vector form).

2. FORMULATION OF THE PROBLEM

Under the assumptions that [1, 2, 9] the tube is made of homogeneous Kelvin–Voigt viscoelastic material, the fluid is incompressible and inviscid, the effect of the pipe motion on the fluid is negligible and the velocity profile of the fluid is uniform over the cross-sectional area of the pipe (i.e., the plug-flow type), the equation of motion for a uniform Bernoulli–Euler pipe is given by [1, 2] (see Figure 1).

$$C_i I \frac{\partial^5 y}{\partial x^4 \partial t} + EI \frac{\partial^4 y}{\partial x^4} + (m_f U^2 + pA - T) \frac{\partial^2 y}{\partial x^2} + 2m_f U \frac{\partial^2 y}{\partial x \partial t} + m_f \frac{\partial U}{\partial t} \frac{\partial y}{\partial x}$$

$$+ C_0 \frac{\partial y}{\partial t} + (m_f + m_p) \frac{\partial^2 y}{\partial t^2} = F(x, t), \tag{1}$$

where x is the axial co-ordinate along the undeformed centerline of the pipe, y the vertical (transverse) deflection of the pipe, E the Young's modulus, A the cross-sectional area of the pipe, I the moment of inertia of A, m_p and m_f are, respectively, the mass of pipe and that of fluid per unit length of the pipe, U the fluid velocity, p the fluid pressure intensity, T the axial tension in the pipe, C_i the coefficient of (internal) dissipation of the pipe material, C_0 the coefficient of external (outer) viscous damping due to friction between the pipe and the fluid, and t the time.

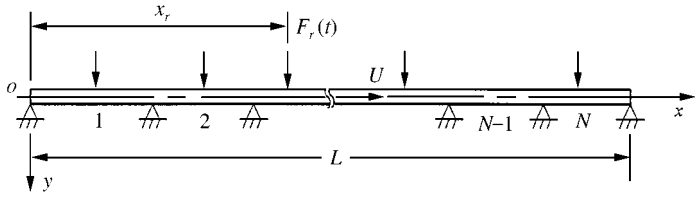

Figure 1. An N-span non-periodically supported fluid-conveying pipe subjected to the external loads $F_r(t)$, $r = 1, 2, \ldots$

According to the modal analysis approach, one may assume that

$$y(x, t) = \sum_{j=1}^{n'} Y_j(x) q_j(t), \tag{2}$$

where $Y_j(x)$ denotes the jth normal mode shape of the multispan pipe containing "stationary" fluid (with $U = 0$), $q_j(t)$ denotes the associated generalized co-ordinate, and n' is the total number of mode shapes considered. For the non-periodic multispan pipe as shown in Figure 1, neither admissible, comparison nor eigenfunction for the normal made shapes is obtainable, hence the "numerical" (or vector) normal mode shapes of the pipe are determined with the TMM in this paper. The transfer matrices for the field, station and intermediate rigid (pin) support are shown in Appendix A.

The substitution of equation (2) into equation (1) gives

$$\begin{aligned} &C_i I \sum_{j=1}^{n'} Y_j''''(x)\dot{q}_j(t) + EI \sum_{j=1}^{n'} Y_j''''(x) q_j(t) + (m_f U^2 + pA - T) \sum_{j=1}^{n'} Y_j''(x) q_j(t) \\ &+ 2m_f U \sum_{j=1}^{n'} Y_j'(x)\dot{q}_j(t) + m_f \dot{U} \sum_{j=1}^{n'} Y_j'(x) q_j(t) + C_0 \sum_{j=1}^{n'} Y_j(x)\dot{q}_j(t) \\ &+ (m_f + m_p) \sum_{j=1}^{n'} Y_j(x)\ddot{q}_j(t) = F(x, t), \end{aligned} \tag{3}$$

where the primes and overdots denote the differentiations with respect to the spatial co-ordinate x and the temporal co-ordinate t respectively.

Multiplying equation (3) by $Y_k(x)\,\mathrm{d}x$, integrating the resulting expression over the total pipe length L, and using the following relationship for the orthogonality of normal mode shapes of the Bernoulli–Euler beam:

$$\int_0^L Y_j(x)\, Y_k(x)\,\mathrm{d}x = \{Y\}_j^{\mathrm{T}} \{Y\}_k \Delta x = \delta_{jk} \Delta x, \tag{4}$$

one obtains

$$\begin{aligned} &(\bar{m}_f + \bar{m}_p)\ddot{q}_k(t) + 2m_f U \left[\sum_{j=1}^{n'} A_{kj}\dot{q}_j(t) \right] + (\bar{C}_i I \lambda_k^4 + \bar{C}_0)\dot{q}_k(t) \\ &+ \left[\left(m_f \dot{U} \sum_{j=1}^{n'} A_{kj} \right) + (m_f U^2 + pA - T) \sum_{j=1}^{n'} B_{kj} + EI\Delta x \cdot \lambda_k^4 \right] \\ &q_k(t) = \bar{F}_k(t), \quad k = 1, 2, \ldots, n', \end{aligned} \tag{5}$$

where

$$\delta_{jk} = \begin{cases} 1{\cdot}0 & \text{if } j = k \\ 0 & \text{if } j \neq k \end{cases} \quad \text{(Kronecker delta)}, \tag{6}$$

$$\bar{m}_f = m_f \Delta x, \quad \bar{m}_p = m_p \Delta x, \quad \bar{C}_i = C_i \Delta x, \quad \bar{C}_0 = C_0 \Delta x, \tag{7}$$

$$\lambda_k = \sqrt[4]{(m_f + m_p)\omega_k^2 / EI}, \qquad \bar{F}_k(t) = \int_0^L F(x,t)\, Y_k(x)\, \mathrm{d}x = \{F(t)\}^{\mathrm{T}} \{Y\}_k, \tag{8, 9}$$

$$A_{kj} = \int_0^L Y_j'(x)\, Y_k(x)\, \mathrm{d}x = \{Y'\}_j^{\mathrm{T}} \{Y\}_k \Delta x \quad (j, k = 1 \sim n'), \tag{10}$$

$$B_{kj} = \int_0^L Y_j''(x)\, Y_k(x)\, \mathrm{d}x = -\frac{1}{EI} \{M\}_j^{\mathrm{T}} \{Y\}_k \Delta x \quad (j, k = 1 \sim n'), \tag{11}$$

$$\begin{aligned} \{F(t)\} &= \{F(x_1, t) \;\; F(x_2, t) \cdots F(x_r, t) \cdots F(x_s, t)\} \\ &= \{F_1(t) \;\; F_2(t) \cdots F_r(t) \cdots F_s(t)\}, \end{aligned} \tag{12}$$

$$\{Y\}_k = \{Y(x_1) \;\; Y(x_2) \cdots Y(x_r) \cdots Y(x_s)\}_k = \{Y_1 \;\; Y_2 \cdots Y_r \cdots Y_s\}_k, \tag{13}$$

$$\{Y'\}_j = \{Y'(x_1) \;\; Y'(x_2) \cdots Y'(x_r) \cdots Y(x_s)\}_j = \{Y_1' \;\; Y_2' \cdots Y_r' \cdots Y_s'\}_j, \tag{14}$$

$$\{Y''\}_j = \{Y''(x_1) \;\; Y''(x_2) \cdots Y''(x_r) \cdots Y''(x_s)\}_j = \{Y_1'' \;\; Y_2'' \cdots Y_r'' \cdots Y_s''\}_j, \tag{15}$$

In the foregoing equations, $\{\ \}$ denotes a column vector, Δx is the length of each "field" between any two adjacent "elastic" stations, s is the total number of elastic stations for the entire multispan pipe with length L and x_r is the location of the rth elastic station. The relationship between Δx and s is given by (see Figure 2(a))

$$s = L/\Delta x \tag{16a}$$

while the relationship between x_r and Δx is given by

$$x_r = [(r - 1) + 0{\cdot}5]\, \Delta x. \tag{16b}$$

In equation (8), ω_k is the kth natural frequency of the multispan pipe filled with the stationary fluid (with $U = 0$) and is obtained from the TMM in this paper. In equation (11), $\{M\}_j$ is the vector of bending moments associated with the jth mode shape $\{Y\}_j$, which is one of the components for the state-variable vector $\{Q\}$ for the TMM as may be seen from equation (A.4). In equation (12), $F_r(t)$ is the concentrated force located at $x = x_r$ (applied on the rth "elastic" station). For the case that no load is applied on station r one has $F_r(t) = 0$, and for the distributed loads one may replace the latter by the equivalent concentrated loads applied on the associated "elastic" stations.

It is noted that neither the curvatures of the mode shapes, $Y_j''(x)$, nor the associated bending moments $M_j(x)$ may be obtained from the conventional FEM unless a particular formulation is employed. This is one of the reasons why TMM is more suitable than the FEM for the evaluation of B_{kj} ($k, j = 1$–n') defined by equation (11) and so is the case for the solution of the title problem.

Writing equation (5) in matrix form gives

$$[\bar{M}]\{\ddot{q}(t)\} + [\bar{C}]\{\dot{q}(t)\} + [\bar{K}]\{q(t)\} = \{\bar{F}(t)\}, \tag{17}$$

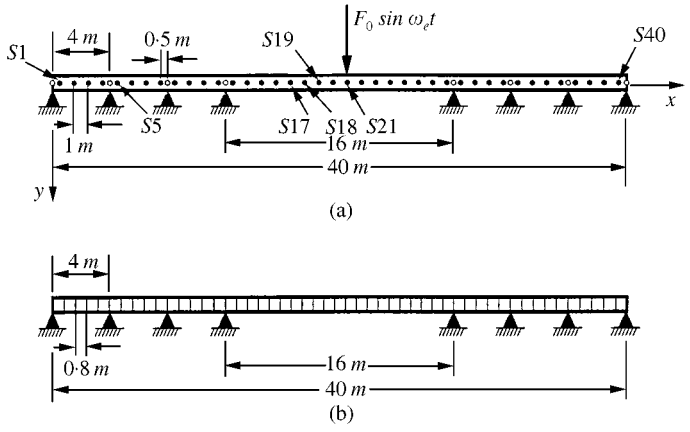

Figure 2. The mathematical models of piping system for (a) the transfer matrix method (TMM) and (b) the finite element method (FEM).

where

$$[\bar{M}] = (\bar{m}_f + \bar{m}_p)\lceil 1 \;\; 1 \cdots 1 \rfloor_{n' \times n'}, \qquad \{q(t)\} = \{q_1(t) \;\; q_2(t) \cdots q_{n'}(t)\}_{n' \times 1}, \tag{18, 19}$$

$$[\bar{C}] = 2m_f U[A] + [\bar{C}]', \qquad [\bar{K}] = m_f \dot{U}[A] + (m_f U^2 + pA - T)[B] + [\bar{E}], \tag{20, 21}$$

$$\{\bar{F}(t)\} = \{\bar{F}_1(t) \;\; \bar{F}_2(t) \cdots \bar{F}_{n'}(t)\}, \qquad [\bar{C}]' = \bar{C}_0 \lceil 1 \;\; 1 \cdots 1 \rfloor + \bar{C}_i I \lceil \lambda_1^4 \;\; \lambda_2^4 \cdots \lambda_{n'}^4 \rfloor, \tag{22, 23}$$

$$[\bar{E}] = EI\Delta x \lceil \lambda_1^4 \;\; \lambda_2^4 \cdots \lambda_{n'}^4 \rfloor. \tag{24}$$

In the above expressions, $\{\ \}$ denotes the column vector, $[\ ]$ the square matrix and $\lceil \quad \rfloor$ the diagonal matrix. In equations (20) and (21), the coefficients of the matrices $[A]$ and $[B]$ are defined by equations (10) and (11) respectively.

For a Bernoulli–Euler tubular beam filled with stationary fluid, one has

$$EI \frac{\partial^4 y}{\partial x^4} + (m_f + m_p) \frac{\partial^2 y}{\partial t^2} = 0. \tag{25}$$

Free vibration of the beam takes the form

$$y(x, t) = Y(x) e^{i\omega t}, \tag{26}$$

where $Y(x)$ denotes the amplitude of $y(x, t)$, which is the mode shape of the beam, ω is the corresponding natural frequency and $i = \sqrt{-1}$. The substitution of equation (26) into equation (25) yields

$$Y''''(x) = \lambda^4 Y(x) \tag{27}$$

where the definition of λ is given by equation (8) for the kth mode.

By using the Newmark direct integration method [22], one may obtain the values of $\{q(t)\}$, $\{\dot{q}(t)\}$ and $\{\ddot{q}(t)\}$ from equation (17). The vector for the vertical (transverse)

displacements of the piping system at any time t, $\{y(t)\}$, is then determined by

$$\{y(t)\} = \sum_{j=1}^{n'} \{Y\}_j q_j(t), \tag{28}$$

where

$$\{y(t)\} = \{y_1(x_1, t)\ \ y_2(x_2, t) \cdots y_r(x_r, t) \cdots y_s(x_s, t)\}$$

$$= \{y_1(t)\ \ y_2(t) \cdots y_r(t) \cdots y_s(t)\}. \tag{29}$$

By setting $[\bar{C}] = 0$ and $\{\bar{F}(t)\} = 0$, one may determine the influence of fluid velocity (U), the Coriolis force term $2m_f U(\partial^2 y/\partial x \partial t)$, fluid pressure intensity (p) and axial tension (T) on the natural frequencies of the piping system from equation (17) with the Jacobi method [22]. If $\{\bar{F}(t)\} = 0$ and $[\bar{C}] \neq 0$, then the "complex" eigenvalues of equation (17) may be determined with the technique of solving the eigenvalues of a "damped" system as shown in reference [21].

3. NUMERICAL RESULTS AND DISCUSSION

The mathematical model for the multispan fluid-conveying piping system studied in this paper is shown in Figure 2(a). The total length of the pipe is $L = 40$ m, the total number of spans is $N_s = 7$. The length of the middle span (the 4th span counted from the left end of the pipe) is $\ell_4 = 16$ m, and all the other six spans have the same lengths $\ell_i = 4$ m ($i = 1, 2, 3, 5, 6, 7$). The whole pipe rests on eight "rigid" supports. For convenience of free-vibration analysis with the TMM, the whole pipe is divided into 47 pipe segments bounded by 48 stations. Each pipe segment between any two adjacent "stations" constitutes a "field". In Figure 2(a), the black points (•) denote the "elastic" stations, while the small hollow circles (○) located above the eight rigid supports are the "elastic" stations, but is impossible for all the "rigid" stations. It is evident that transverse deflection (in the y direction) is possible for all the "rigid" stations. All fields have the same lengths $\Delta x = 1{\cdot}0$ m except those bounded by an elastic station and a rigid station. The length for each of the latter fields is $\Delta x' = \Delta x/2 = 0{\cdot}5$ m. Since the lumped masses on the rigid stations have no effect on the natural frequencies and the associated mode shapes of the pipe, these lumped masses are set to be equal to zero. In other words, the total mass of the whole pipe is divided into 40 lumped masses and concentrated on the 40 "elastic" stations. The magnitude of each lumped mass is equal to $(m_f + m_p)\Delta x$. In Figure 2(a), the notation Si denotes the ith "elastic" stations (excluding the "rigid" stations). To check the results obtained from the TMM, free-vibration analysis on the "stationary" pipe is also made by using the FEM. Figure 2(b) shows the finite element model.

The other pertinent data are: outside diameter of pipe $d_o = 355{\cdot}6$ mm, thickness of pipe wall $t_w = 9{\cdot}0$ mm, inside diameter of pipe $d_i = d_o - 2t_w = 337{\cdot}6$ mm, cross-sectional area $A = \pi d_i^2/4 = 8{\cdot}95 \times 10^{-2}$ m^2, moment of inertia for the cross-sectional area $I = \pi(d_o^4 - d_i^4)/64 = 1{\cdot}4726 \times 10^{-4}$ m^4, Young's modulus $E = 200 \times 10^9$ N/m^2, mass of pipe per unit length $m_p = 76{\cdot}9$ kg/m, mass of fluid per unit length $m_f = \rho_f A = 89{\cdot}5$ kg/m, pipe length $L = 40$ m, internal fluid pressure intensity $p = 3000$ N/m^2, axial tension in the pipe $T = 0$, damping coefficients per unit length $C_0 = C_i = 198{\cdot}8256$ (N-s/m)/m. The values of C_0 and C_i are determined based on the assumption that

$$C_0 = C_i = 2\xi'(m_f + m_p)\omega_1 \tag{30}$$

TABLE 1

The five lowest undamped natural frequencies of the "stationary" piping system (with $U = p = T = 0$*),* ω_i $(i = 1\text{–}5)$*, obtained from TMM and FEM*

Methods	Natural frequencies (rad/s)				
	ω_1	ω_2	ω_3	ω_4	ω_5
TMM	29·87164	84·62074	167·52000	259·28000	273·98390
FEM	29·87839	84·62407	167·59460	259·54270	274·21770

with damping parameter $\xi' = 0{\cdot}02$ and the first undamped natural frequency of the "stationary" pipe, ω_1, as shown in Table 1. The total number of modes considered is $n' = 5$. It has been found that the differences between the results based on $n' = 5$ and those based on $n' > 5$ are negligible.

3.1. UNDAMPED NATURAL FREQUENCIES AND MODE SHAPES OF THE STATIONARY PIPE

For the present "stationary" piping system (with $U = p = T = 0$), the five lowest "undamped" natural frequencies and the corresponding normal mode shapes obtained from TMM (with the mathematical model shown in Figure 2(a)) and FEM (with the mathematical model shown in Figure 2(b)) are listed in Table 1 and plotted in Figure 3 respectively. From Table 1 one sees that the five lowest undamped natural frequencies ω_i $(i = 1\text{–}5)$ obtained from the TMM and FEM are in close agreement. The corresponding mode shapes $\{Y\}_i$ $(i = 1\text{–}5)$ obtained from the TMM (denoted by ——) are also very close to those from the FEM (denoted by ----) as shown in Figure 3.

3.2. EFFECT OF AVERAGE FLUID VELOCITY U_0 ON THE UNDAMPED NATURAL FREQUENCIES

If the "instantaneous" fluid velocity in the pipe takes the form $U(t) = U_0(1 + \delta \cos \omega_f t)$, where U_0 denotes the "average" fluid velocity (or simply called fluid velocity), δ denotes the pulsating parameter and ω_f is the pulsating frequency, then the influence of U_0 on the five lowest undamped natural frequencies of the piping system under the conditions that $\delta = p = T = [\bar{C}] = 0$ is shown in Table 2. Since $\delta = 0$, the magnitude of ω_f has nothing to do with the natural frequencies $\bar{\omega}_i$ $(i = 1, 2, \ldots)$. The third row of Table 2 shows the five lowest natural frequencies of the piping system with $U = U_0 = 0$, which are exactly equal to the ones listed in the third row of Table 1. In other words, the five lowest undamped natural frequencies $\bar{\omega}_i$ $(i = 1\text{–}5)$ obtained from the "numerical" mode method agree with the corresponding ones ω_i $(i = 1\text{–}5)$ obtained from the TMM if $U = \delta = p = T = [\bar{C}] = 0$ as it should be. For convenience, the relationship between U_0 versus $\bar{\omega}_i$ $(i = 1\text{–}3)$ is also shown in Figure 4, which is plotted based on the data listed in columns 1–4 of Table 2. From Figure 4 one sees that increasing fluid velocity U_0 has the effect of reducing the undamped natural frequencies of the piping system, $\bar{\omega}_i$ $(i = 1, 2, \ldots)$, and this effect of U_0 on the first natural frequency $\bar{\omega}_1$ is much more significant than that on the other ones $\bar{\omega}_i$ $(i = 2, 3, \ldots)$. Besides, the value of $\bar{\omega}_1$ approaches zero when $U_0 \approx 55$ m/s (see Figure 4). This means that the present piping system will have the problem of buckling instability [3, 4] if the fluid velocity U_0 is greater than 55 m/s in the specified conditions.

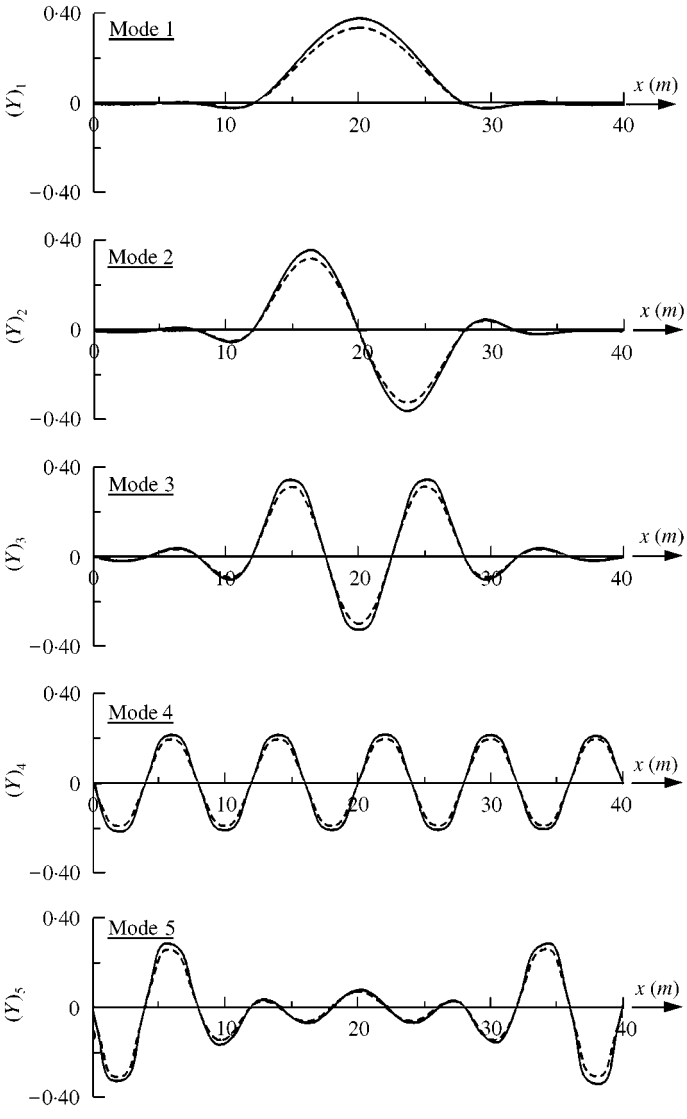

Figure 3. The five lowest normal mode shapes of the stationary piping system, $\{Y\}_i$ ($i = 1$–5), obtained from TMM (———) and those from FEM (-----).

3.3. TIME HISTORIES OF VERTICAL DISPLACEMENTS FOR STATION No. 19

Unless particularly stated, the dynamic responses of the piping system presented in this paper are obtained based on the assumptions that $p = 3000\ \text{N/m}^2$, $\delta = T = 0$, damping parameter $\xi' = 0{\cdot}02$ (or $C_0 = C_i = 198{\cdot}8256$ (N-s/m)/m), and a single exciting force on "elastic" station No. 21 (located at $x_{21} = 20{\cdot}5$ m) $F_{21}(t) = 9800 \sin \omega_e t$ N. Under the last conditions and with Coriolis force considered and fluid velocity $U_0 = 5$ m/s, the time histories of the vertical (transverse) displacements for the "elastic" station No. 19 (located at $x_{19} = 18{\cdot}5$ m) of the piping system as shown in Figure 2(a) are plotted in Figure 5 for the exciting frequencies $\omega_e = 20$, 30, 50, 84 and 120 rad/s, respectively, where the abscissa denotes the time t (s) and the ordinate denotes the vertical displacements of station No. 19 at

TABLE 2

Influence of average fluid velocity U_0 on the five lowest undamped natural frequencies of the piping system with $\delta = p = T = [\bar{C}] = 0$

Fluid velocity U_0 (m/s)	Natural frequencies $\bar{\omega}_i$ (rad/s)				
	$\bar{\omega}_1$	$\bar{\omega}_2$	$\bar{\omega}_3$	$\bar{\omega}_4$	$\bar{\omega}_5$
0·0	29·87164	84·62074	167·52000	259·28000	273·98390
10·0	29·38198	84·37637	167·37799	259·18592	273·89179
20·0	27·85883	83·63878	166·95142	258·89916	273·61957
30·0	25·10894	82·39430	166·23842	258·41020	273·17559
40·0	20·63445	80·61865	165·23594	257·70157	272·57529
50·0	12·70060	78·27453	163·93953	256·74959	271·83950
60·0	− 12·80547	75·30732	162·34330	255·52526	270·99355
70·0	− 23·48067	71·63761	160·43966	253·99643	270·06498

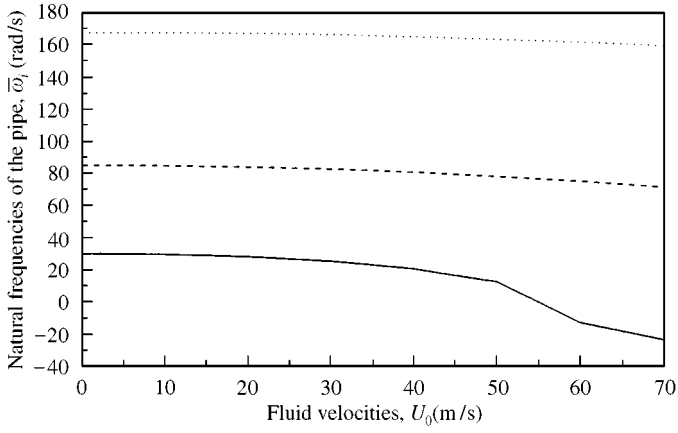

Figure 4. Effect of average fluid velocity U_0 on the three lowest undamped natural frequencies of the piping system with $\delta = p = T = [\bar{C}] = 0$: ——— for $\bar{\omega}_1$; ----- for $\bar{\omega}_2$; ····· for $\bar{\omega}_3$.

any time t, $y_{19}(t)$, with unit meters. From the figure one sees that the two curves based on $\omega_e = 30$ rad/s (denoted by –△–) and $\omega_e = 84$ rad/s (denoted by ----) oscillate sinusoidally with amplitudes increasing gradually with the increase of time. This is a resonable result, because the last two exciting frequencies (ω_e) are near the first undamped natural frequency $\bar{\omega}_1 = 29{\cdot}73535$ rad/s and the second one $\bar{\omega}_2 = 84{\cdot}55239$ rad/s (with $p = 3000$ N/m^2 and $U_0 = 5$ m/s) respectively. However, the other three curves based on the exciting frequencies $\omega_e = 20$, 50 and 120 rad/s oscillate irregularly because these exciting frequencies are far away from any natural frequencies of the piping system. Perhaps, all the foregoing facts may be helpful for confirming the reliability of the results presented in the subsequent subsections.

3.4. EFFECT OF FLUID VELOCITY U_0 ON THE MAXIMUM DYNAMIC RESPONSES

If all the situations are the same as in the last subsection except that the Coriolis force is neglected and the exciting frequencies are $\omega_e = 0$–300 rad/s, then the influence of the fluid

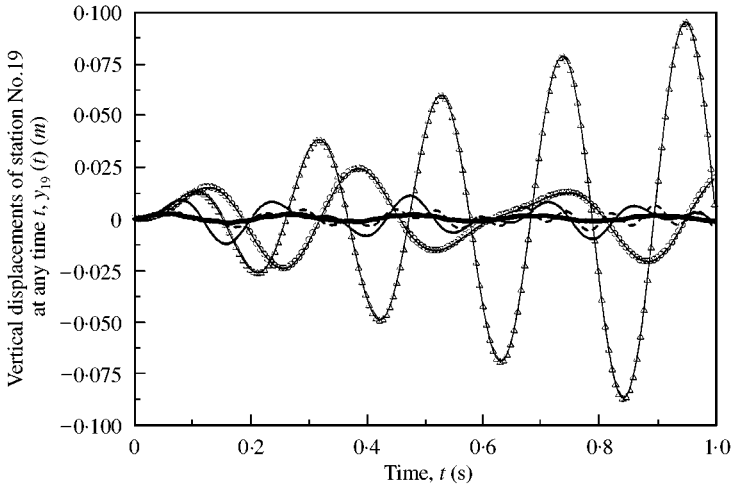

Figure 5. Time histories of vertical (transverse) displacements of station No. 19 for the piping system, $y_{19}(t)$, subjected to $F_{21}(t) = 9800 \sin \omega_e t$ N with $U_0 = 5$ m/s: —○— for $\omega_e = 20$ rad/s, —△— for $\omega_e = 30$ rad/s, ——— for $\omega_e = 50$ rad/s, ----- for $\omega_e = 84$ rad/s, ▬▬ for $\omega_e = 130$ rad/s.

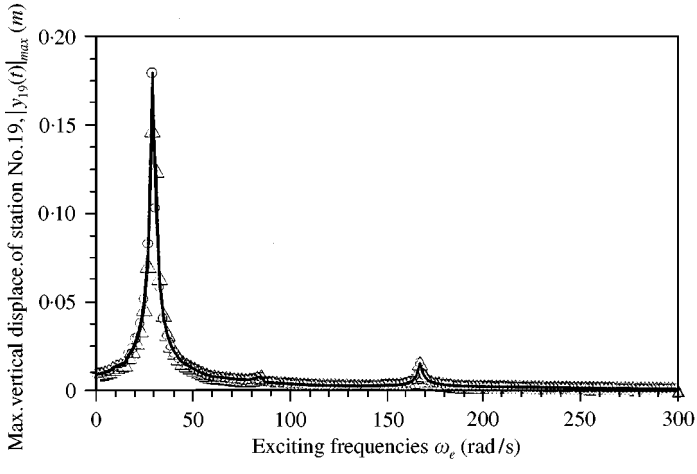

Figure 6. Influence of fluid velocity U_0 on the maximum vertical displacements of station No. 19 of the piping system, $|y_{19}(t)|_{max}$, with the Coriolis force neglected: —△— for $U_0 = 0$; ----- for $U_0 = 5$ m/s; —○— for $U_0 = 10$ m/s.

velocity U_0 on the maximum vertical (transverse) displacements of station No. 19 of the piping system (see Figure 2(a)), $|y_{19}(t)|_{max}$, is shown in Figure 6 for the cases of $U_0 = 0$, 5 and 10 m/s respectively. It is seen that the first peak value of $|y_{19}(t)|_{max}$ corresponding to $\omega_e \approx 30$ rad/s $\approx \bar{\omega}_1$ increases with increasing fluid velocity U_0 and all the values of $|y_{19}(t)|_{max}$ corresponding to the other exciting frequencies are hardly affected by the fluid velocity U_0. This phenomenon is similar to the influence of U_0 on the undamped natural frequencies of the piping system, $\bar{\omega}_i$ $(i = 1, 2, \ldots)$, where the first natural frequency $\bar{\omega}_1$ is significantly dependent upon the magnitude of U_0, while the other natural frequencies $\bar{\omega}_i$ $(i = 2, 3, \ldots)$ are less dependent on the fluid velocity U_0 as shown in the previous subsection (see Figure 4).

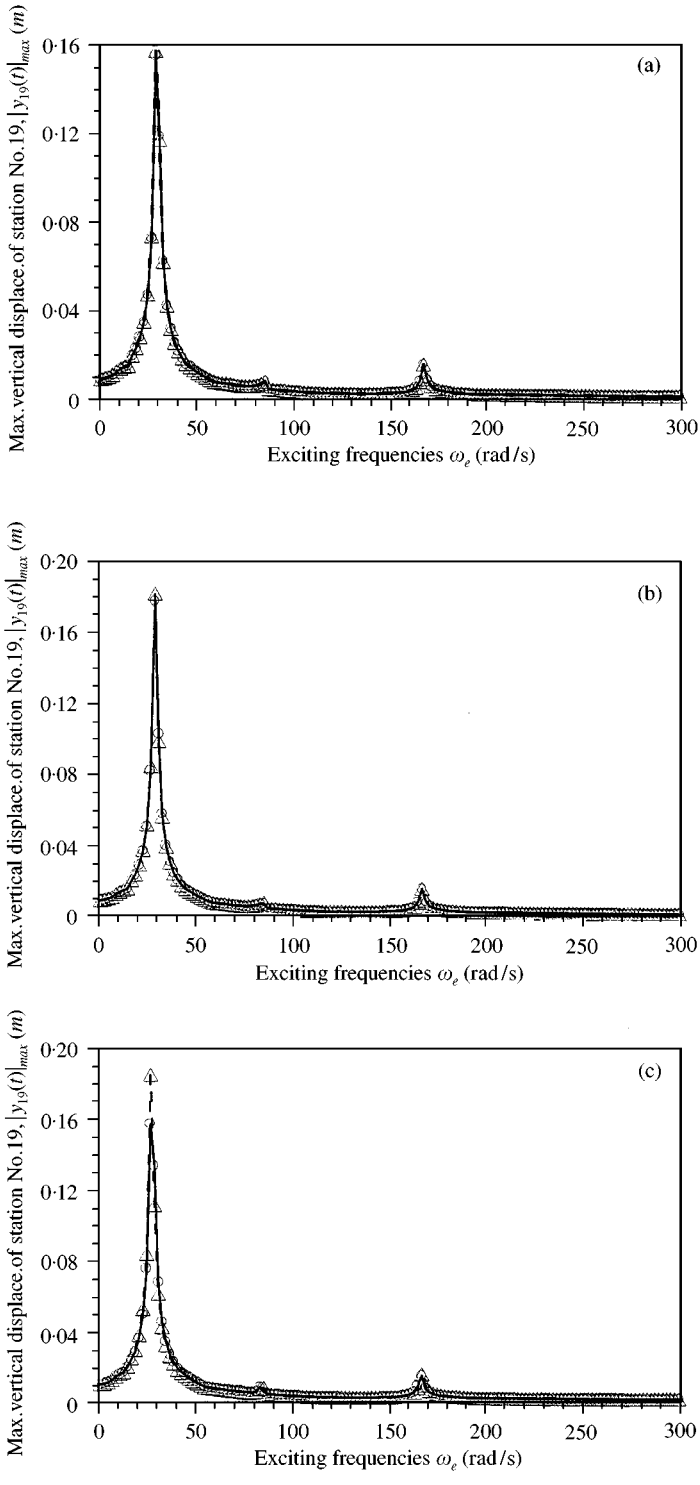

Figure 7. Influence of Coriolis force on the maximum vertical displacements at station No. 19 of the piping system, $|y_{19}(t)|_{max}$, for (a) fluid velocity $U_0 = 5$ m/s, (b) $U_0 = 10$ m/s and (c) $U_0 = 20$ m/s: —○— with the Coriolis force neglected: -△- with Coriolis force considered.

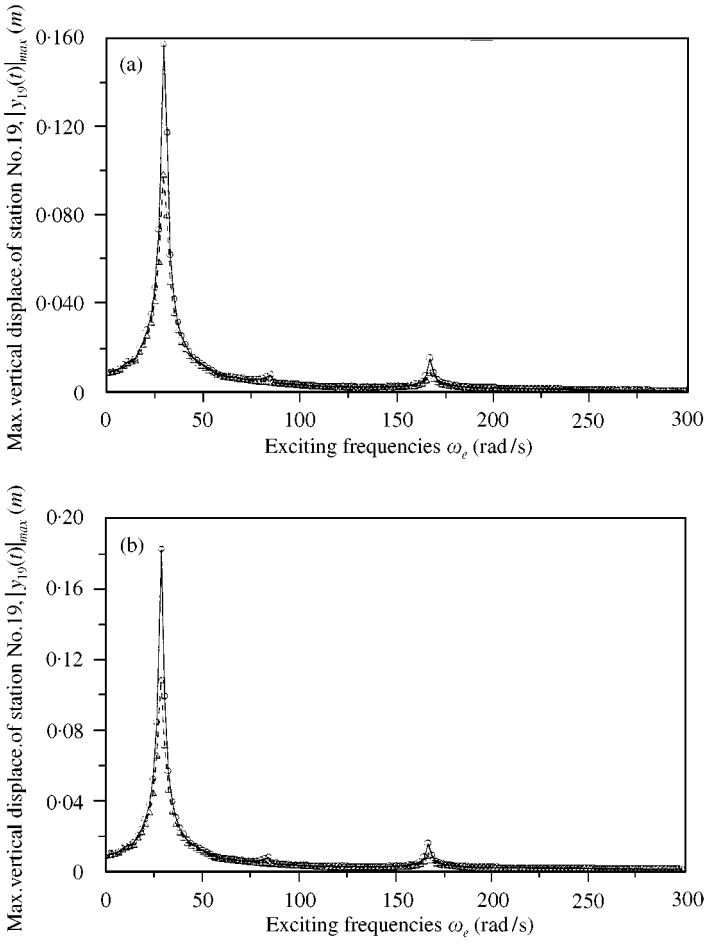

Figure 8. Influence of damping parameter ξ' on the maximum vertical displacements of station No. 19 for the piping system with Coriolis force considered for (a) $U_0 = 5$ m/s and (b) $U_0 = 10$ m/s: —○— with $\xi' = 0{\cdot}02$; -△-- with $\xi' = 0{\cdot}04$.

3.5. EFFECT OF CORIOLIS FORCE ON THE MAXIMUM DYNAMIC RESPONSES

For the present problem, the Coriolis force is represented by the term $2m_f U\,\partial^2 y/\partial x \partial t$ of equation (1) or $2m_f U[A]$ of equation (20). If all conditions are the same as in the last subsection except the Coriolis force and the fluid velocities, then the effect of Coriolis (damping) force on the maximum response of station No. 19, $|y_{19}(t)|_{max}$, is shown in Figure 7 where the solid curves are obtained by "neglecting" the Coriolis force and the dashed curves by "considering" the Coriolis force. Besides, Figure 7(a) is for the case of fluid velocity $U_0 = 5$ m/s, Figure 7(b) for $U_0 = 10$ m/s and Figure 7(c) for $U_0 = 20$ m/s. From Figure 7(a) one sees that the Coriolis force has negligible damping effect (to suppress the dynamic response of the piping system) over the range of exciting frequencies $\omega_e = 1$–300 rad/s. The effect of the Coriolis force as shown in Figures 7(b) and 7(c) is similar to that shown in Figure 7(a) except that the differences between the first peak values of $|y_{19}(t)|_{max}$ for the curves of Figures 7(b) and 7(c) corresponding to the small triangles (△) and those corresponding to the small hollow circles (○) increase with the increase of fluid velocities U_0. This means that the Coriolis force has the "negative" damping effect (to raise the

dynamic response of the piping system) if $\omega_e \approx 30$ rad/s $\approx \bar{\omega}_1$. In reference [4], it has been reported that the interplay between the centrifugal and Coriolis forces may lead to an overall "negative" damping. It is believed that this should be the reason for arriving at the last phenomenon.

3.6. EFFECT OF DAMPING ON THE MAXIMUM DYNAMIC RESPONSES

Under the same conditions as in the previous subsections with the Coriolis force considered, the influence of damping parameter ξ' (or damping coefficients per unit length C_0 and C_i defined by equation (30)) on the maximum response of station No. 19, $|y_{19}(t)|_{max}$, is shown in Figure 8(a) for fluid velocity $U_0 = 5$ m/s and in Figure 8(b) for $U_0 = 10$ m/s, where the solid curves denote the result based on $\xi' = 0{\cdot}02$ and the dashed curves denote that based $\xi' = 0{\cdot}04$. It is seen that the values of $|y_{19}(t)|_{max}$ associated with the dashed curves (with $\xi' = 0{\cdot}04$) are always smaller than the corresponding ones associated with the solid curves (with $\xi' = 0{\cdot}02$) as it should be.

4. CONCLUSIONS

1. For the dynamic analyses of a long "non-periodic" multispan fluid-conveying pipe undergoing various excitations, the presented "numerical" (or vector) mode approach incorporated with the transfer matrix method provides one of the most simple, straightforward and practical techniques in addition to the conventional finite element method.
2. By neglecting the damping effects due to inner damping (of material), outer damping and Coriolis force, the natural frequencies of the piping system decrease with increasing (average) fluid velocity U_0, and buckling instability of the first mode may occur if U_0 exceeds a certain value.
3. If the effect of the Coriolis force is neglected, then the maximum dynamic responses of a piping system due to an excitation with exciting frequency ω_e near the first natural frequency of the system ($\bar{\omega}_1$) will significantly increase with increasing the fluid velocity U_0.
4. The Coriolis force has a negligible effect on the dynamic response of a piping system with lower fluid velocities, but it has a "negative" damping effect to raise the dynamic response of the piping system with higher fluid velocities. In general, this "negative" effect significantly increases with increasing fluid velocities (U_0) only if the exciting frequency (ω_e) approaches the first natural frequency of the piping system ($\bar{\omega}_1$).

REFERENCES

1. S. S. CHEN 1971 *Journal of the Engineering Mechanics Division, Proceedings of the American Society of Civil Engineers* **97**, 1469–1485. Dynamic stability of a tube conveying fluid.
2. M. P. PAIDOUSSIS and N. T. ISSID 1974 *Journal of Sound and Vibration* **33**, 267–294. Dynamic stability of pipes conveying fluid.
3. E. C. TING and A. HOSSEINIPOUR 1986 *Journal of Sound and Vibration* **88**, 289–298. A numerical approach for flow-induced vibration of pipe structures.
4. M. P. PAIDOUSSIS, T. P. LUU and B. E. LAITHIER 1986 *Journal of Sound and Vibration* **106**, 311–331. Dynamics of finite-length tubular beams conveying fluid.
5. W. H. CHEN and C. N. FAN 1987 *Journal of Sound and Vibration* **119**, 429–442. Stability analysis with lumped mass and friction effects in elastically supported pipes conveying fluid.

6. A. PRAMILA, J. LAUKKANEN and S. LIUKKONEN 1991 *Journal of Sound and Vibration* **144**, 421–425. Dynamics and stability of short fluid-conveying Timoshenko element pipes.
7. C. O. CHANG and K. C. CHENG 1994 *Journal of Pressure Vessel Technology* **116**, 57–66. Dynamics and stability of pipes conveying fluid.
8. J. BRATT 1995 *Structure Engineering Review* **7**, 15–21. Lateral vibration of fluid-conveying pipes.
9. R. A. STEIN and M. W. TOBRINER 1970 *Transactions of the ASME, Journal of Applied Mechanics* **37**, 906–916. Vibration of pipes containing flowing fluids.
10. K. SINGH and A. K. MALLIK 1977 *Journal of Sound and Vibration* **54**, 55–66. Wave propagation and vibration response of a periodically supported pipe conveying fluid.
11. K. SINGH and A. K. MALLIK 1979 *Journal of Sound and Vibration* **62**, 379–397. Parametric instabilities of a periodically supported pipe conveying fluid.
12. G. H. KOO and Y. S. PARK 1998 *Journal of Sound and Vibration* **210**, 53–68, Vibration reduction by using periodic supports in piping system.
13. D. J. MEAD and A. K. MALLIK 1976 *Journal of Sound and Vibration* **47**, 457–471. An approximate method of predicting the response of periodically supported beams subjected to random convected loading.
14. U. N. RAO and A. K. MALLIK 1977 *Journal of Sound and Vibration* **55**, 395–403. Response of finite periodic beams to convected loading—an approximate method.
15. A. S. DMITRIEV 1982 *Soviet Applied Mechanics* **18**, 179–186. Dynamics of continuous multispan beams under a moving force.
16. J. S. WU and C. W. DAI 1987 *Journal of Structural Engineering*, ASCE **113**, 458–474, Dynamic response of multispan nonuniform beam due to moving loads.
17. C. W. CAI, Y. K. CHEUNG and H. C. CHAN 1988 *Journal of Sound and Vibration* **123**, 461–472. Dynamic response of infinite continuous beams subjected to moving force—an exact method.
18. K. HENCHI, M. FAFARD, G. DHATT and M. TALBOT 1997 *Journal of Sound and Vibration* **199**, 33–50. Dynamic behavior of multispan beams under moving loads.
19. R. W. CLOUGH and J. PENZIEN 1976 *Dynamics of Structures*, New York: McGraw-Hill.
20. W. D. PILKEY and P. Y. CHANG 1978 *Modern Formulas for Statics and Dynamics*. New York: McGraw-Hill.
21. L. MEIROVITCH 1967 *Analytical Methods in Vibrations*. London: Macmillan.
22. K. J. BATHE 1982 *Finite Element Procedures in Engineering Analysis*. Englewood Cliffs, NJ: Prentice-Hall, Inc.

APPENDIX A: TRANSFER MATRICES FOR THE BERNOULLI–EULER BEAM

For a Bernoulli–Euler beam, the transfer matrix for the rth field, $[T_F]_r$, that for the rth station, $[T_s]_r$, and that for the kth intermediate rigid (pin) support as shown in Figure 1,

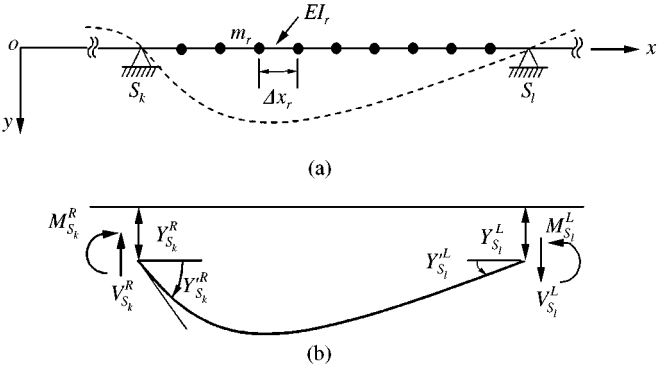

Figure A.1. Diagram for determination of transfer matrix of rigid-supported stations: (a) discrete system for beam segment between any two adjacent supports S_k and S_l; (b) state variables at the right side of support S_k and the left side of support S_l.

$[T_S]_{S_k}$, are given by [16, 20]

$$[T_F]_r = \begin{bmatrix} 1 & -\Delta x_r & -\dfrac{\Delta x_r^2}{2EI_r} & -\dfrac{\Delta x_r^3}{6EI_r} \\ 0 & 1 & \dfrac{\Delta x_r^2}{EI_r} & \dfrac{\Delta x_r^2}{2EI_r} \\ 0 & 0 & 1 & \Delta x_r \\ 0 & 0 & 0 & 1 \end{bmatrix}, \quad [T_S]_r = \begin{bmatrix} 1 & 0 & 0 & 0 \\ 0 & 1 & 0 & 0 \\ 0 & 0 & 1 & 0 \\ -\omega^2 m_r & 0 & 0 & 1 \end{bmatrix}, \quad \text{(A.1, 1.2)}$$

$$[T_S]_{S_k} = \begin{bmatrix} 1 & 0 & 0 & 0 \\ 0 & 1 & 0 & 0 \\ 0 & 0 & 1 & 0 \\ -\dfrac{T_{11}^{kl}}{T_{14}^{kl}} & -\dfrac{T_{12}^{kl}}{T_{14}^{kl}} & -\dfrac{T_{13}^{kl}}{T_{14}^{kl}} & 0 \end{bmatrix}, \quad \text{(A.3)}$$

where Δx_r and I_r, respectively, denote the length and moment of inertia for the rth field (beam segment), m_r denotes the lumped mass for the rth station, and T_{1j}^{kl} ($j = 1$–4) denote the coefficients of the first row of the cumulative transfer matrix for the stations and fields located at the space between the two adjacent intermediate rigid supports S_k and S_l (see Figure A1).

The corresponding state vector for equations (A.1)–(A.3) is

$$\{Q\} = \{Y \;\; Y' \;\; M \;\; V\}, \quad \text{(A.4)}$$

where Y, Y', M, V denote the vertical (transverse) displacement, slope, shear force and bending moment at any section of the beam (see Figure A1) respectively.